Engineered Living Materials for Bioproduction Downstream Processing

Sarah Browning[1], Davide Prati[2], Paolo Magni[2], Lorenzo Pasotti[2], and Sara Molinari[1,3]*

[1] Fischell Department of Bioengineering, University of Maryland College Park, College Park, MD, USA
[2] Department of Electrical, Computer and Biomedical Engineering, University of Pavia, 27100 Pavia, Italy
[3] Department of Chemical and Biomolecular Engineering, University of Maryland College Park, College Park, MD, USA

**Corresponding Author:* saramol@umd.edu

Abstract

Microbial fermentation provides a renewable route to a wide portfolio of fuels, chemicals, and therapeutics, yet product recovery is still dominated by energy-intensive biomass-removal operations. Here, we engineered *Escherichia coli* to display elastin-like polypeptides on its outer membrane, transforming single cells into flocculating *E. coli*-based engineered living materials (FloEc-ELMs). These self-assembling aggregates span from micrometer to centimeter scale, sediment within two hours, and do not compromise the ethanol-production capacity of an industrial ethanologenic strain. When deployed in bench-scale lactose fermentations, FloEc-ELMs reduced filtration time 3.2-fold, while preserving an ethanol yield comparable to the non-engineered parental strain. By mapping ELP sequence polarity to toxicity and aggregate size, and by porting the system across genetic backgrounds and inducible promoters, we provide design rules for modular, portable ELM-mediated flocculation that can streamline downstream processing in large-scale biomanufacturing.

Keywords: engineered living materials; *E. coli*; elastin-like polypeptides; flocculation; bioprocess intensification; downstream processing

---

1. Introduction

Synthetic biology provides a powerful framework for designing and optimizing microbial systems capable of converting raw materials into a broad spectrum of valuable products, including biofuels, pharmaceuticals, and food ingredients[1–4]. Unlike traditional chemical synthesis methods, which often rely on petroleum-derived feedstocks,

engineered microbes offer a sustainable alternative by utilizing renewable or waste-derived substrates[5,6]. Among microbial platforms, *Escherichia coli* remains a workhorse due to its rapid growth rate (doubling time ~20 minutes), minimal nutrient requirements, and well-characterized metabolic and genetic toolkits[7,8]. These attributes have enabled *E. coli* to be extensively engineered for a wide range of applications, including the synthesis of non-native compounds, enhancement of native metabolic pathways, broadening of substrate utilization, and increased robustness for operation in challenging environments such as industrial waste streams[9–15].

Despite these advancements, downstream processing, particularly biomass separation, remains a major obstacle to the scalability and economic viability of microbial bioproduction[16]. Whether the target product is intracellular or secreted, biomass recovery is often necessary to separate product-rich cells from spent medium or to remove cells from supernatant containing the final product. This step is both capital- and energy-intensive. Common methods such as centrifugation and filtration require costly infrastructure and high operational input[17–20]. Moreover, filtration units are susceptible to membrane fouling, necessitating frequent cleaning or replacement, and can also compromise cell viability, a critical factor for reinoculation or continuous processing[21]. For example, cross-flow microfiltration, though widely used, can cause shear-induced cell lysis that limits reuse[21].

To address these limitations, microbial flocculation has emerged as a promising alternative[20,22]. Flocculation enables cells to aggregate into large aggregates that sediment rapidly under gravity, greatly simplifying biomass separation and reducing the reliance on mechanical or membrane-based methods. This approach has the potential to reduce or eliminate the costs associated with biomass harvesting and allow for smaller, less complex separation units. Control over cellular aggregation would therefore directly benefit downstream processing and overall process economics. Notably, some yeast strains, such as *Saccharomyces cerevisiae,* naturally exhibit flocculation, which has been leveraged in industrial bioethanol production to facilitate cell removal[23]. In addition, flocculating yeasts are used as immobilized biocatalysts in continuous processes, enabling high cell density fermentation and enhanced productivities[24].

In contrast, *E. coli* lacks native flocculation ability under standard growth conditions. Several strategies have been explored to overcome this limitation, including: (i) genetic induction of flocculation by overexpressing native genes such as the cellulose synthase subunit BcsB[25]; (ii) chemical flocculation using multivalent cations, synthetic polymers, or bio-based agents[26]; and (iii) physical methods that damage the outer membrane, such as treatment with

cerium nitrate or electric fields[26]. While these approaches improve broth clarification, they come with trade-offs. For example, cellulose-mediated flocculation requires supplementation with glucose or other sugars, diverting resources away from product biosynthesis. Moreover, cellulose production imposes a metabolic burden, and the system is not portable; it only functions in strains with an intact *bcs* operon. Similarly, chemical flocculants introduce additional costs and may contaminate the process stream.

Engineered living materials (ELMs) offer a promising and integrative alternative[27,28]: By genetically programming *E. coli* to display interaction domains, such as leucine zippers, nanobody-antigen pairs, or curli-based fusion proteins[29–31], researchers have demonstrated the formation of self-assembling cellular assemblies that are stable, sediment quickly, and retain permeability to small molecules. These designs enable autonomous material formation without exogenous inputs. More recently, work in *Caulobacter crescentus* has shown that elastin-like polypeptides (ELPs)[32], peptides capable of multivalent interactions, can be displayed on the cell surface to drive large-scale assembly[33]. This strategy points toward a scalable, genetically encodable solution to biomass recovery with built-in functional material properties.

Here, we demonstrated the generation of flocculating *E. coli*-based engineered living materials (FloEc-ELMs) by displaying ELPs on the surface of *E. coli* that have a size distribution ranging from micrometers to centimeters. We then implemented FloEc-ELMs in the ethanologenic W105Fe strain optimized for lactose fermentation[34], showing the portability of this technology to a non-laboratory strain and investigating the conditions in which sedimentation could be triggered. Ethanol production performance was not affected by the formation of FloEc-ELMs, and sedimentation markedly shortened the filtration time at the end of batch fermentations.

2. Methods

2.1 Strains and plasmids

All the laboratory strains used in this work for characterizing ELMs are derivatives of *E. coli* BL21, referred to as wild-type. For fermentation experiments and FloEc-ELM formation under ethanol production conditions, the W105Fe ethanologenic strain was used.[34] W105Fe is a derivative of *E. coli* W (DSM 1116), engineered for optimized ethanol production from lactose-rich dairy waste by i) the chromosomal insertion of a constitutive codon-optimized *adhB-pdc* operon (coding for an alcohol dehydrogenase II and a pyruvate decarboxylase), ii) the removal of the *ldhA, frdA,* and

pflB genes that compete with the ethanol production route from pyruvate, and iii) the increase of ethanol tolerance by adaptive evolution.

2.2 Plasmid Assembly

Plasmids for the surface display of ELPs were constructed from the base Addgene plasmid #186314. We replaced the displayed peptide with the fusion construct SpyTag-ELP. Plasmids have been assembled using Golden Gate Assembly[35] to obtain a scarless final sequence. Every plasmid was fully sequenced through Oxford Nanopore Technologies (service provided by Plasmidsaurus). Upon verification, plasmids were transformed into *E. coli* strains. Specific ELP sequences are reported in the Supplementary Section 1.3.

2.3 Cell growth

Engineered and wild-type *E. coli* cells were grown by inoculating a single colony into 3 mL of LB medium in 14 mL culture tubes. For the ethanologenic strain, LB media was supplemented with α-lactose at a concentration of 2 g/L. All cultures were grown overnight at 37 °C, in shaking conditions (250 rpm). The overnight culture was inoculated in fresh media at a 1:100 dilution into either 14 mL tubes (final volume: 7 mL) or 125 mL glass flask (final volume: 50 mL). Cultures were grown until reaching log phase (Optical Density—OD600: 0.4-0.6) and then induced by (Isopropyl β-d-1-thiogalactopyranoside—IPTG, or N-3-oxohexanoyl-L-homoserine lactone—HSL) at the indicated concentration. Sedimentation assays, flow cytometry, and confocal microscopy started after cultures grew under shaking conditions for 2 h after induction. FlowCam analysis and imaging of macroscopic particles in flasks have been performed after an overnight induction.

2.4 Confocal microscopy

To verify the correct extracellular localization of ELPs, engineered cells were collected via centrifugation at 4000 rpm for 1 minute and resuspended in 1 mL 0.01M phosphate-buffered saline (PBS). This step was repeated twice. Washed cells were incubated with 80 µg of SpyCatcher-GFP for 60 min at 30 °C to allow for the formation of the SpyTag-SpyCatcher covalent bonds[33]. Samples were then washed three times with 1 mL 0.01 M PBS and placed between a slab of PBS agarose (1.5% w/v) and a glass coverslip. For imaging, we used the Olympus FLUOVIEW FV3000 Confocal Laser Scanning Microscope. Data was acquired using the FLUOVIEW software and analyzed using Fiji software.

2.5 Flow cytometry

Flow cytometry was used to quantify ELP display. For the former assay, cells were incubated with SpyCatcher-GFP as described in Section 2.4. Cells were then washed three times with 1 mL 0.01M PBS. A total of 10,000 events were recorded for each sample using a BD FACSCelesta flow cytometer. Data acquisition was performed using BD FACSDiva software, and analysis was performed using FlowJo software.

2.6 Viability Assay

To assess viability of engineered and wild-type cells, we performed propidium iodide (PI) staining. Cells induced for 2 h were collected via centrifugation at and resuspended in 1mL 0.01 M PBS. This step was repeated twice. 200 µL of washed culture was put into a new 1.5 mL tube for staining. Samples were combined with 10 µLof PI (ThermoFisher) and shaken on a Corning LSE Platform rocker for 15 minutes to allow for the PI to permeate into dead cells. Cells were imaged with confocal microscopy as described in Section 2.4.

2.7 Sedimentation assay of ELMs

Sedimentation assays were performed as described in Trunk *et al*.[36]. Specifically, cells were grown in tubes, as described in section 2.3. After 2 h of induction, cell cultures were incubated at 37 °C statically. Every hour, we measured the OD600 by sampling 200 µL of culture from the top of the tube and diluting it into 800 µL of fresh LB. Sedimentation curves were plotted in GraphPad Prism. All curves were normalized to the average OD600 value at t=0.

2.8 Particle analysis of ELMs

To assess the relationship between ELP composition and FloEc-ELM size distribution, particle analysis of the ELMs was performed using flow imaging microscopy with FlowCam. FlowCam 8100 (Yokogawa Fluid Imaging Technologies) configured with a 2X objective, 5 mL syringe, and FOV 1000 flow cell was used to capture high-resolution images of FloEc-ELMs between 40 µm and 1000 µm. Cultures were grown in flasks as described in section 2.3. After 15 hours, cultures were diluted 1:10 in 1X PBS to ensure clarity for particle analysis. Before analysis, all FloEc-ELMs larger than the detection limit (1000 µm) were removed from the culture samples with a pipette. Samples (~20 mL) were manually primed into the FlowCam microfluidic flow cell and processed using AutoImage Mode in consecutive 2 mL readings at a 4 mL/min flow rate. Particles were defined by dark pixels only at a segmentation threshold of 20. To filter out cellular debris and small particulates, a 40 µm capture filter was included in the image acquisition context settings. Data acquisition and analysis were performed with VisualSpreadsheet 6 software provided by Yokogawa Fluid Imaging Technologies.

2.9 Fermentation experiments

Batch fermentation experiments were carried out in test tubes in high-oxygen conditions as described previously[37]. Pre-cultures of ethanologenic strains were inoculated with single colonies and grown at 37°C, 220 rpm for 16 h in 5 mL of LB Lennox supplemented with 40 g/L lactose in 50-mL conical tubes. The cultures were 100-fold diluted in 5 mL of LB Lennox with 40 g/L lactose and 100 mM phosphate buffer at pH 7.0, and incubated under the same conditions as above for 24 h. When indicated, after 2 h from the dilution, HSL was added at a 2 nM concentration to trigger the assembly of FloEc-ELMs in the plasmid-bearing strains. Samples were withdrawn at t=0 h and t=24 h, filtered (0.2 µm) and stored at –20°C before the quantification of fermentation products. At the end of fermentation, a sedimentation assay was performed to assess flocculation in the cultures induced with HSL, using an Infinite F200Pro plate reader (Tecan) to measure OD600 in 200-µl samples.

2.10 Quantification of sugars and ethanol

A high-performance liquid chromatography system (LC-2000 HPLC, Jasco) was used to detect the residual lactose and produced ethanol at the end of fermentation experiments. An autosampler was used to inject 25 µL of samples, which were analyzed with a refractive index detector (RID, Shimadzu). The Supelco C-610H 30 cm × 7.8 mm column (59320-U, Sigma Aldrich), kept at 30°C, and the 0.1% H_3PO_4 mobile phase at the 0.5 mL/min flow rate were used for the analyses[37]. Quantifications were carried out from the measured chromatograms by the ChromNAV 2.0 software (Jasco). Ethanol titer (*i.e.*, the concentration at the end of the experiment) and conversion yield were used as fermentation performance indexes. The conversion yield was computed as a percentage of the maximum theoretical yield, considering that the maximum ethanol production corresponds to 0.538 grams of ethanol per gram of consumed lactose[37]. Apart from lactose, no other sugars were detected in fermentation samples.

2.11 Filtration assay

A 20-fold scale-up (100 mL culture in a 250-mL flask) of the fermentation test described in Section 2.7 was performed for the W105Fe strain and the W105Fe_ELP_LYS_{10}strain in which the assembly of FloEc-ELM was induced by 2 nM HSL as described above. At the end of fermentation, cultures were transferred into 100-mL cylinders and left at 37°C for 1.5 h to allow for sedimentation. A 75-mL volume was then taken from the non-sedimented fraction and loaded into a 250-mL vacuum filtration unit with a 0.22-µm PES membrane (Biofil). Vacuum was applied by a diaphragm mini-pump (PM20405-86, VWR International GmbH) with a maximum pressure of 2.4 bar and a vacuum

of 250 mbar. The time needed to filter 50 mL and 75 mL was recorded. The flow rate was computed as 75 mL divided by the time needed to complete the filtration.

2.12 Statistical analysis

All comparisons done between three or more groups were performed using the Brown-Forsythe and Welch ANOVA. All ANOVAs had multiple comparisons post hoc analysis (Dunnett T3) performed. For comparisons with less than three groups, a two-tailed Welch's t test was used. In all cases, a p-value (p) cutoff of 0.05 was used to identify statistically significant differences. In the graphs, **** = $p<0.0001$, ** = $p<0.01$, and * = $p<0.05$.

3. Results

3.1 Formation of FloEc-ELMs via Surface Display of ELPs on E. coli

Building upon previous research in *C. crescentus*[33], we engineered FloEc-ELMs by ELPs on the surface of *E. coli*. ELPs consist of repetitive pentapeptides (Val-Pro-Gly-X-Gly), where the guest residue (X), typically Valine, can be replaced by any other natural amino acid, excluding Proline[32]. Previous studies demonstrated that replacing guest residues with Alanine improves bacterial expression[38] and surface display in *E. coli*, facilitating cell-cell adhesion[39]. Based on this, we created a 10-repeat ELP construct (referred to as ELP-ALA_{10}), containing six Alanine substitutions, fused to the EhaA autotransporter for extracellular display[29] (Fig. 1A). For effective characterization, a C-terminal SpyTag[40] and an N-terminal His-Tag were included in the construct. This construct was placed under the control of an IPTG-inducible promoter (T5/lac), which allows for the fine regulation of gene expression in *E. coli*[41].

Successful extracellular localization of ELP-ALA_{10} was confirmed via confocal microscopy, using SpyCatcher-GFP to specifically bind the SpyTag[33], resulting in distinct fluorescent halos around cells expressing intracellular mScarlet (red fluorescence protein) from a separate plasmid (Fig. 1B). In contrast, cells incubated with SpyTag–GFP do not show any green fluorescent staining (Fig. 1B—left panel), confirming that the extracellular fluorescence observed (Fig. 1B—right panel) is due to specific SpyCatcher–SpyTag recognition. Western blot analyses, performed with anti-HisTag antibody, validated the integrity and correct molecular weight of ELP-ALA_{10} (~46.17 kDa), with strong enrichment in the outer membrane fractions (Supplementary Fig. 1), consistent with surface display. Flow cytometry provided quantitative confirmation of these findings, showing significantly (two orders of

magnitude) higher fluorescence intensity in SpyCatcher-GFP stained samples compared to SpyTag-GFP (Supplementary Fig. 2).

To evaluate the efficiency of FloEc-ELMs in facilitating biomass separation, a central goal of this study, we conducted sedimentation assays to quantify deposition kinetics (Fig. 1C). Cells were cultivated in shaking conditions and induced during mid-log phase (OD600 0.4–0.6). Two hours after the induction, we incubated the cells statically to allow for deposition. This time point was selected based on the average duration required for protein transcription, translation, and translocation to the cell surface; we confirmed that the level of surface-displayed protein after 2 hours matched that observed after overnight induction (Supplementary Fig. 2). To determine the optimal expression level of ELP-ALA_{10}, we compared sedimentation at various IPTG concentrations. Complete settling of ELMs was achieved after 2 hours of static incubation, with a final OD of 0.188, in contrast to the higher residual ODs of 0.892 and 0.869 observed for non-induced and non-transformed controls, respectively (Fig. 1C). The most efficient sedimentation occurred at 25 μM IPTG, while increasing the inducer concentration to 250 μM provided no further benefit. These results identify 25 μM IPTG as the optimal induction level, effectively promoting rapid FloEc-ELM deposition while minimizing unnecessary metabolic burden.

Ensuring cell viability is essential for deploying FloEc-ELMs in bioproduction, as cells must retain full metabolic activity throughout the process. To assess viability, we used propidium iodide (PI), a dye that selectively stains cells with compromised outer membranes[42]. Confocal microscopy revealed that ELP-ALA_{10} surface display substantially reduced viability, evident from a markedly higher proportion of red-fluorescent cells (Fig. D—right panel, and Supplementary Fig. 3) relative to the wild-type strain (Fig. D—left panel, and Supplementary Fig. 3). This observation was further supported by the frequent appearance of elongated cell morphologies, indicative of cellular stress (Fig. D, and Supplementary Fig. 3). While confocal imaging provides qualitative insight, quantitative analysis via flow cytometry, the standard method for PI-based viability assays[42], is not suitable here due to measurement bias introduced by large cellular aggregates[43]. Taken together, these results confirm that ELP surface display drives the formation of FloEc-ELMs that enhance sedimentation efficiency relative to wild-type cells. However, this benefit is accompanied by a notable reduction in cell viability, presenting a critical trade-off for downstream applications.

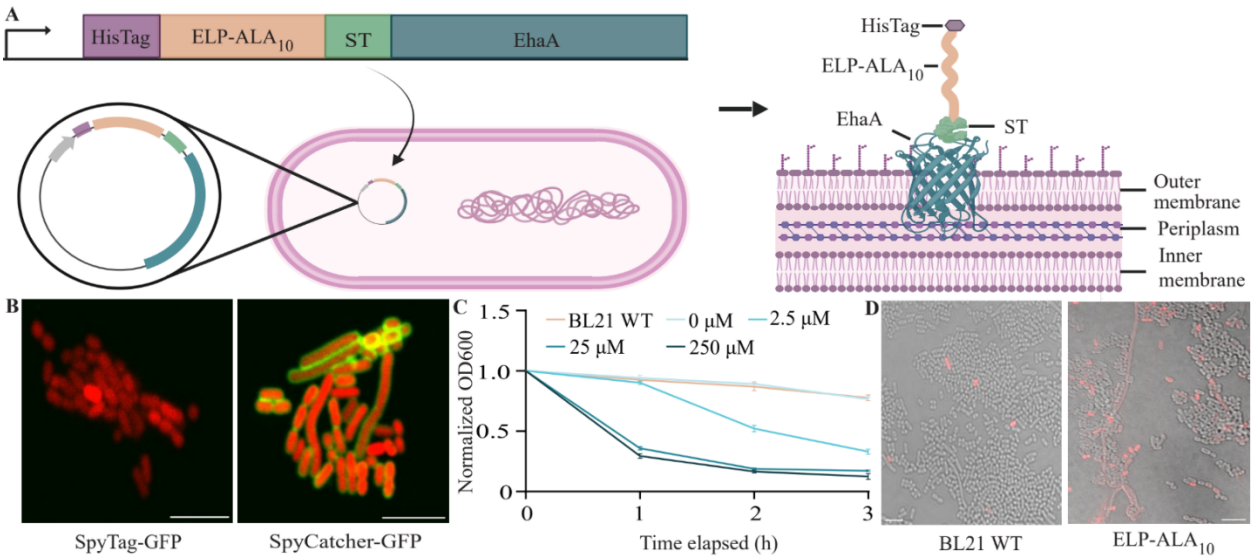

Figure 1. Surface display of ELPs yields FloEc-ELMs. A) Schematic of the ELP-ALA$_{10}$ expression cassette and the intended surface display mechanism using the EhaA autotransporter[29]. **B)** Confocal microscopy images of *E. coli* cells displaying ELP-ALA$_{10}$ stained with SpyTag-GFP (left panel) or SpyCatcher-GFP (right panel). **C)** Sedimentation assay of ELP-ALA$_{10}$ FloEc-ELMs induced with increasing concentrations of IPTG. OD600 values were normalized to 1 at t = 0. Error bars are plotted around the mean and represent 95% confidence intervals of six samples. **D)** Confocal microscopy of cells displaying ELP-ALA$_{10}$ induced with 25 μM IPTG and stained with PI to assess cell viability. Scale bars are 5 μm.

3.2 Polarity-Driven Optimization of ELPs Enhances Viability and Enables Scalable FloEc-ELM Formation

We hypothesized that the elevated toxicity associated with ELP-ALA$_{10}$ stemmed in part from the high hydrophobicity of its peptide chains, potentially leading to nonspecific interactions with the lipid bilayer and resulting in outer membrane destabilization[44]. To mitigate this effect, we designed two alternative ELP variants in which Alanine was substituted with either positively charged Lysine (ELP-LYS$_{10}$) or negatively charged Glutamic Acid (ELP-GLU$_{10}$), introducing increased polarity. To evaluate surface display, we performed GFP–SpyCatcher staining followed by flow cytometry. All constructs exhibited comparable levels of display (Fig. 2A), although ELP-ALA$_{10}$ and ELP-GLU$_{10}$ showed elevated green fluorescence signals likely influenced by nonspecific GFP interactions, as indicated by the high background in the SpyTag-GFP-stained negative control (Fig. 2A). Importantly, PI staining revealed substantially reduced toxicity in both polar constructs, ELP-LYS$_{10}$ and ELP-GLU$_{10}$, compared to ELP-ALA$_{10}$

(Fig. 2B, and Supplementary Fig. 3), reinforcing the hypothesis that hydrophobicity plays a central role in membrane-associated cytotoxicity. Among the tested variants, ELP-LYS_{10} best preserved cell viability (Fig. 2B, and Supplementary Fig. 3), emerging as the most promising candidate for further engineering.

Remarkably, cells displaying either ELP-LYS_{10} or ELP-GLU_{10} formed macroscopic FloEc-ELMs, extending up to several centimeters in length, when cultured in Erlenmeyer flasks (Fig. 2C—central and right panels, and Supplementary Fig. 4). In contrast, ELP-ALA_{10}-expressing cells failed to form visible aggregates under the same conditions (Fig. 2C—left panel, and Supplementary Fig. 4). Among the polar variants, ELP-GLU_{10} yielded the largest observed FloEc-ELMs, reaching approximately 5.8 cm in length, though this phenotype was inconsistently reproduced, indicating high variability (Fig. 2C, and Supplementary Fig. 4). To further quantify aggregation at the microscopic scale (2 μm to 1 mm), we used FlowCam 8000 to analyze the size distribution of FloEc-ELMs across the three constructs. ELP-LYS_{10} produced the largest mean particle diameter (68.05 ± 1.08 μm), though not significantly different from ELP-ALA_{10} (Fig. 2D). Interestingly, ELP-GLU_{10} resulted in the smallest average diameter (57.19 ± 2.57 μm) within this range, despite its superior macroscopic aggregation. These results suggest a broad size distribution for ELP-GLU_{10}, with fewer mid-sized aggregates and occasional formation of very large structures. Aggregate count analysis further supported this interpretation: ELP-LYS_{10} produced the fewest aggregates, consistent with its larger size (Supplementary Figs. 5 and 6), while ELP-GLU_{10} displayed highly variable particle counts, aligning with its more unpredictable large-scale aggregation behavior.

Sedimentation assays mirrored these trends, showing that both polar constructs facilitated more efficient cell deposition than ELP-ALA_{10}, as indicated by a final OD of ~0.143, representing a 23.94% improvement over the alanine-substituted construct (Fig. 2E). Based on these findings, we selected ELP-LYS_{10} for further experimentation. Although ELP-GLU_{10} performed comparably in many respects, ELP-LYS_{10} was favored due to its more consistent aggregation profile and superior impact on cell viability.

Western blot analysis confirmed the expected molecular weight of ELP-LYS_{10} and its enrichment in the membrane fraction (Supplementary Fig. 7), similar to ELP-ALA_{10}. Notably, ELP-LYS_{10} showed reduced cytosolic presence (Supplementary Fig. 7), which may further contribute to its improved viability. Together, these findings

underscore the advantages of polar substitutions in ELP design, both for enhancing cell viability and enabling the formation of robust, large-scale FloEc-ELMs suitable for scalable bioprocessing.

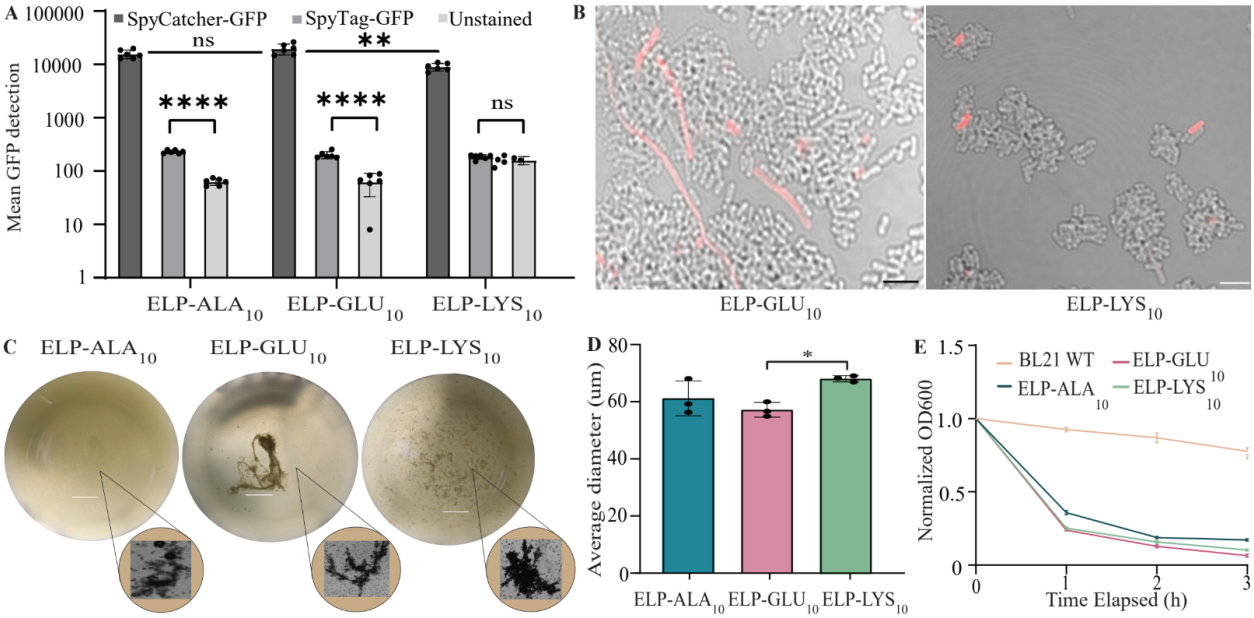

Figure 2. ELP polarity affects FloEc-ELM size and viability. A) Fluorescent flow cytometry of the ELP-displaying cells stained with SpyCatcher-GFP. Error bars are centered on the mean value and represent 95% confidence intervals of six samples. **B)** Confocal microscopy of cells displaying ELP-GLU$_{10}$ (left panel) and ELP-LYS$_{10}$ (right panel) induced with 25 µM IPTG and stained with PI to assess cell viability. **C)** Photographs of FloEc-ELMs grown overnight in culture flasks, showing macroscopic aggregation above the detection limit of the FlowCam. In the zoomed-in area beneath the flask bottom are pictures of the corresponding microscopic aggregates captured by the FlowCam. **D)** Average particle diameter of FloEc-ELMs engineered through the display of different ELP sequences. Error bars are centered on the mean value and represent 95% confidence intervals of three samples. **E)** Sedimentation assay comparing the deposition rates of different FloEc-ELMs induced with 25 µM IPTG. While ELP-GLU$_{10}$ and ELP-LYS$_{10}$ did not have a significant difference, they were both significantly lower than ELP-ALA$_{10}$ ($p=0.0003$). OD600 values were normalized to 1 at $t = 0$. Error bars are centered on the mean value and represent 95% confidence intervals of six samples.

3.3 Transferring FloEc-ELM Technology to an Ethanol-Producing E. coli Strain for Tunable Flocculation in Fermentation Settings

To demonstrate the potential of FloEc-ELMs for enhancing biomass separation during lactose fermentation, we adapted the ELP-LYS_{10} display system for use in the ethanologenic *E. coli* strain W105Fe[34]. Because the original IPTG-inducible promoter is also activated by lactose—present in the fermentation medium—its use would result in constitutive, non-tunable expression of ELP-LYS_{10} under these conditions. To circumvent this limitation, we refactored the system to be controlled by an HSL/LuxR inducible circuit derived from the *Aliivibrio fischeri* quorum-sensing system[45]. In this design, a constitutive promoter drives expression of the LuxR transcriptional regulator, which binds its cognate ligand N-3-oxohexanoyl-L-homoserine lactone (HSL) upon diffusion into the cell. The resulting LuxR–HSL complex activates transcription from the P_{lux} promoter, thereby enabling controlled induction of ELP-LYS_{10}. All tests in this section were conducted in LB medium supplemented with 2 g/L lactose to simulate fermentation-relevant conditions.

Sedimentation assays were conducted across a range of HSL concentrations to evaluate the inducibility of FloEc-ELMs in the W105Fe strain (Fig. 3A). Induction with 2 nM HSL efficiently triggered FloEc-ELM formation, achieving aggregation levels comparable to those observed in BL21 cells induced with IPTG. Increasing the HSL concentration to 20 or 200 nM did not further enhance sedimentation, suggesting that 2 nM is sufficient for maximal FloEc-ELM assembly. Confocal microscopy-based PI staining confirmed that both the non-flocculating W105Fe control and the 2 nM HSL-induced W105Fe–ELP-LYS_{10} strain exhibited similar low levels of red fluorescence (Fig. 3B), indicating physiological levels of cell death under these conditions. In contrast, cells induced with 20 nM HSL displayed more frequent elongation and a much greater proportion of PI-stained cells, suggesting that overexpression of the surface-displayed protein disrupts membrane integrity and interferes with normal cell division. Based on these results, we selected 2 nM HSL as the optimal induction level for subsequent experiments, balancing robust flocculation with preserved cell viability.

To further characterize ELP-LYS_{10} surface expression in W105Fe, we performed SpyCatcher-GFP staining and particle size analysis. Flow cytometry revealed that W105Fe–ELP-LYS_{10} cells displayed significantly lower surface fluorescence than their BL21 counterparts (Supplementary Fig. 8), consistent with known differences in genetic background. In particular, BL21 strains are optimized for extracellular protein expression due to the deletion

of the outer membrane protease OmpT[46], which likely contributes to higher surface display levels. In contrast, W105Fe's reduced display may be attributed to protease activity, strain-specific differences in plasmid regulation, transcription or translation efficiencies, or membrane composition changes resulting from ethanol tolerance adaptations[47]. This lower expression level in W105Fe was reflected in its aggregation profile, with FloEc-ELMs exhibiting a smaller average diameter (47.52 ± 0.77 µm) and a reduced particle count (mean: 1,937 particles/mL; Supplementary Figs. 9 and 10) compared to BL21. Nonetheless, despite these differences, W105Fe–ELP-LYS$_{10}$ achieved even more efficient sedimentation than BL21, supporting its suitability for biomass recovery in fermentation contexts. These findings demonstrate that the FloEc-ELM platform can be effectively transferred across *E. coli* strains, yielding consistent flocculation performance and preserving cellular viability.

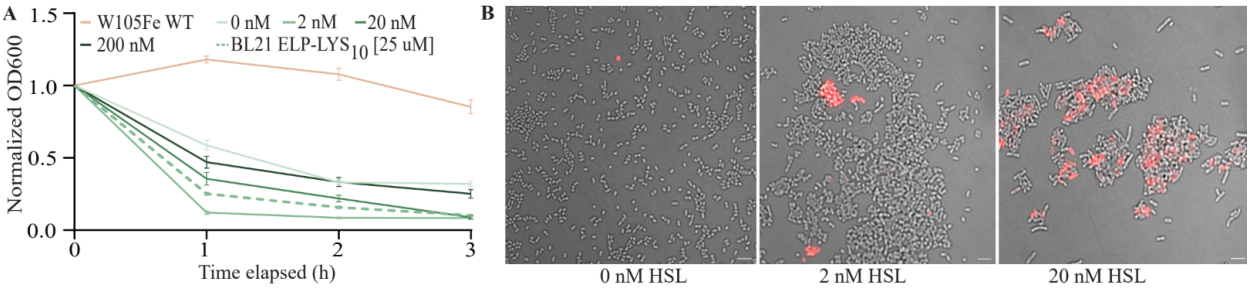

Figure 3. Characterization of FloEc-ELMs engineered in the ethanologenic strain W105F. A) Sedimentation assay showing the rates of FloEc-ELM deposition across the HSL induction range (0, 2, 20, and 200 nM) for the W105Fe WT and W105Fe-ELP-LYS$_{10}$. The dashed line represents the ELP-LYS$_{10}$ system in BL21 for comparison between strains. OD600 values were normalized to 1 at t = 0. Error bars are centered on the mean value and represent 95% confidence intervals of six samples. **B)** Confocal images showing the viability of W105Fe-ELP-LYS$_{10}$ cells at 0 nM (left panel), 2 nM (middle panel), and 20 nM induction (right panel). Scale bars are 5 µm.

3.4 FloEc-ELMs enables efficient ethanol production and biomass recovery in fermentation settings

The ethanologenic W105Fe strain, engineered with the HSL-inducible ELP-LYS$_{10}$ FloEc-ELM system, was evaluated in lactose fermentation experiments to assess two key aspects: whether FloEc-ELM formation affects ethanol production and whether it enhances biomass recovery. We first examined whether FloEc-ELM assembly could be initiated during the stationary phase, at the end of fermentation. No sedimentation was observed under these conditions, likely due to nutrient depletion limiting protein expression and surface display (Supplementary Fig. 11). In contrast, efficient FloEc-ELM formation and sedimentation occurred across a range of initial cell densities when cultures were diluted into fresh medium (Supplementary Fig. 11), suggesting that active growth and nutrient

availability are prerequisites for successful induction. Based on these findings, we initiated FloEc-ELM expression two hours after inoculation, during exponential growth, anticipating that flocculation would remain stable and functional throughout the fermentation period (t = 24 h), facilitating post-process sedimentation. Batch fermentations were conducted using the parental W105Fe wild-type strain and W105Fe harboring the ELP-LYS_{10} system, either uninduced or induced with 2 nM HSL. All fermentations were performed in medium containing 40 g/L lactose to ensure sustained ethanol production. Ethanol titers measured at the end of fermentation were comparable across all strains (Fig. 4A), with final concentrations of approximately 17.5 g/L, representing 80% of the maximum theoretical yield and indicating complete lactose consumption. These high yields reflect previously reported values for non-flocculating control strains[37], indicating that FloEc-ELM formation does not impair ethanol productivity.

We next evaluated post-fermentation sedimentation under static conditions. The induced FloEc-ELM strain achieved a 90% reduction in cell density in the supernatant, whereas the non-flocculating parental strain showed only a 29% decrease (Fig. 4B). The non-induced W105Fe-ELP-LYS_{10} strain exhibited an intermediate reduction of 50%, likely due to leaky expression from the inducible promoter. These results demonstrate that FloEc-ELMs remain active throughout the fermentation process, effectively enhancing biomass sedimentation without compromising product yield.

To determine whether improved sedimentation translates into more efficient biomass recovery, we performed a follow-up fermentation using W105Fe and W105Fe-ELP-LYS_{10} induced with 2 nM HSL. After fermentation, cultures were statically incubated for 1.5 hours to allow aggregate settling, followed by filtration of the supernatants. No filter clogging occurred under either condition, and the full 75 mL volume was successfully processed. However, filtration efficiency differed markedly between strains: the FloEc-ELM-forming culture exhibited a 3.2-fold increase in flow rate (9 mL/min) compared to the non-flocculating control (2.9 mL/min) (Fig. 4C). Moreover, the FloEc-ELM condition yielded more consistent filtration rates across replicates, suggesting enhanced process robustness. These findings highlight the practical benefits of FloEc-ELMs for industrial fermentation, including faster broth clarification, reduced equipment load, and potentially lower costs related to membrane cleaning or replacement. In addition to facilitating biomass recovery for reuse, improved clarification also aids in the safe containment of genetically modified organisms prior to downstream ethanol purification.

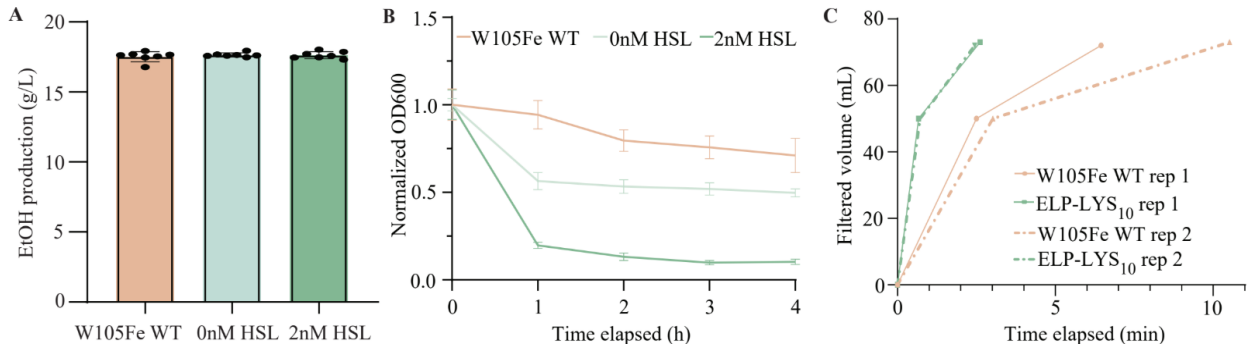

Figure 4. FloEc-ELMs assembly does not impair ethanol production and an increase in biomass recovery. A) Ethanol production quantification showing ethanol titers are not significantly different between W105Fe WT, induced W105Fe-ELP-LYS_{10}, and non-induced W105Fe-ELP-LYS_{10} cells. OD600 values were normalized to 1 at t = 0. Error bars are centered on the mean value and represent 95% confidence intervals of seven samples. **B)** Sedimentation assay conducted after a 24-hour batch fermentation. Error bars are centered on the mean value and represent 95% confidence intervals of three samples. **C)** Filtered volume over time of the W105Fe WT and W105Fe-ELP-LYS_{10} strain. The graph shows two replicates for each W105Fe strain.

4. Discussion

Our data establish that the extracellular display of repeating ELP motifs is sufficient to convert planktonic *E. coli* into self-assembling, gravity-settling engineered living materials. Increasing peptide polarity sharply decreased PI uptake and filamentation, indicating that excessive hydrophobicity destabilizes the outer membrane, whereas charged guest residues mitigate toxicity. Surprisingly, the negatively charged sequence (ELP-GLU_{10}) produced sporadic centimeter-scale gels despite forming the smallest 2–1000 µm aggregates, suggesting that other nonspecific interactions, such as the electrostatic bonds with the outer surface, may affect higher-order assembly. Host background also influenced display efficiency and aggregate morphology, underscoring the role of surface proteins, like proteases, and membrane composition.

Because ELP display is encoded on a single plasmid and functions under both IPTG and LuxR/HSL promoters, the system is readily integrated into diverse genetic programs. Unlike *bcsB*-based flocculation, which requires an intact chromosomal cellulose operon and diverts carbon from the product pathway, FloEc-ELMs impose minimal metabolic load and are portable across strains. In W105Fe the system retained activity despite reduced display levels, highlighting a forgiving design space that can be optimized for specific hosts.

Crucially, FloEc-ELMs did not compromise ethanol productivity, meeting a primary requirement for deployment in production strains. Rapid sedimentation and the resulting 3.2-fold increase in filtration throughput point to tangible operational savings: smaller filter areas, longer membrane lifetimes, and lower energy consumption. Beyond ethanol, the approach could be extended to any process where the product resides in the broth and biomass reuse, or containment is desirable.

The proof-of-principle could be leveraged for further engineering of FloEc-ELMs, aimed at discovering novel design rules for cellular aggregation, transferring this system into non-model microbial hosts, and developing adaptive control loops that trigger aggregation only once a metabolic or sensor threshold is reached. This could expand the applicability of FloEc-ELMs beyond bioprocessing, where high local cellular concentration and containment may provide advantages.

---

5. Acknowledgements

We thank Dr Birthe Kjellerup (UMD) for FlowCam guidance and Michela Casanova (Univ. Pavia) for fermentation support. SM acknowledges the Army Research Lab (grant no. W911NF-23-2-0040) for supporting this study. PM and LP acknowledge MUR—M4C2 1.5 of PNRR (grant ECS00000036, NODES project).

---

6. References

1. Brooks, S. M. & Alper, H. S. Applications, challenges, and needs for employing synthetic biology beyond the lab. *Nat Commun* **12**, 1390 (2021).
2. Ezeako, E. C., Nwiloh, B. I., Odo, M. C. & Ozougwu, V. E. Harnessing synthetic biology for sustainable industrial innovation: Advances, challenges, and future direction. *Biochemical Engineering Journal* **221**, 109777 (2025).
3. Voigt, C. A. Synthetic biology 2020–2030: six commercially-available products that are changing our world. *Nat Commun* **11**, 6379 (2020).

4. Cowan, A. E., Klass, S. H., Winegar, P. H. & Keasling, J. D. Microbial production of fuels, commodity chemicals, and materials from sustainable sources of carbon and energy. *Current Opinion in Systems Biology* **36**, 100482 (2023).

5. de Lorenzo, V. *et al.* The power of synthetic biology for bioproduction, remediation and pollution control. *EMBO reports* **19**, e45658 (2018).

6. Carruthers, D. N. & Lee, T. S. Translating advances in microbial bioproduction to sustainable biotechnology. *Front. Bioeng. Biotechnol.* **10**, (2022).

7. Pontrelli, S. *et al. Escherichia coli* as a host for metabolic engineering. *Metabolic Engineering* **50**, 16–46 (2018).

8. Valle, A. & Bolívar, J. Escherichia coli, the workhorse cell factory for the production of chemicals. in *Microbial Cell Factories Engineering for Production of Biomolecules* 115–137 (Elsevier, 2021).

9. Wang, C., Pfleger, B. F. & Kim, S.-W. Reassessing *Escherichia coli* as a cell factory for biofuel production. *Current Opinion in Biotechnology* **45**, 92–103 (2017).

10. Liang, L., Liu, R., Freed, E. F. & Eckert, C. A. Synthetic Biology and Metabolic Engineering Employing Escherichia coli for C2–C6 Bioalcohol Production. *Front. Bioeng. Biotechnol.* **8**, (2020).

11. Zhao, C., Zhang, Y. & Li, Y. Production of fuels and chemicals from renewable resources using engineered *Escherichia coli*. *Biotechnology Advances* **37**, 107402 (2019).

12. Rodriguez, A. *et al.* Engineering Escherichia coli to overproduce aromatic amino acids and derived compounds. *Microbial Cell Factories* **13**, 126 (2014).

13. Balola, A., Ferreira, S. & Rocha, I. From plastic waste to bioprocesses: Using ethylene glycol from polyethylene terephthalate biodegradation to fuel *Escherichia coli* metabolism and produce value-added compounds. *Metabolic Engineering Communications* **19**, e00254 (2024).

14. Gao, D., Luan, Y., Wang, Q., Liang, Q. & Qi, Q. Construction of cellulose-utilizing Escherichia coli based on a secretable cellulase. *Microbial Cell Factories* **14**, 159 (2015).

15. Wargacki, A. J. *et al.* An Engineered Microbial Platform for Direct Biofuel Production from Brown Macroalgae. *Science* **335**, 308–313 (2012).

16. Janković, T., Straathof, A. J. & Kiss, A. A. A perspective on downstream processing performance for recovery of bioalcohols. *Journal of Chemical Technology & Biotechnology* **99**, 1933–1940 (2024).

17. Panaksri, A., Kuncharin, P., Wongsirichot, P. & Tanadchangsaeng, N. Coagulation–Flocculation for Polyhydroxyalkanoate Downstream Processing. *Ind. Eng. Chem. Res.* **63**, 15188–15197 (2024).

18. Gottschalk, U. Overview of Downstream Processing in the Biomanufacturing Industry. in *Comprehensive Biotechnology* 698–711 (Elsevier, 2011).

19. Shanu, K., Choudhary, S., Kumari, S., Anu, K. & Devi, S. Downstream Processing for Bio-product Recovery and Purification. in *Recent Advances in Bioprocess Engineering and Bioreactor Design* 139–169 (Springer Nature Singapore, Singapore, 2024).

20. Wang, Y., Ling, C., Chen, Y., Jiang, X. & Chen, G.-Q. Microbial engineering for easy downstream processing. *Biotechnology Advances* **37**, 107365 (2019).

21. Bhave, R. R. Cross-Flow Filtration. in *Fermentation and Biochemical Engineering Handbook* 271–347 (Elsevier, 1996).

22. Mubarak, M., Shaija, A. & Suchithra, T. V. Flocculation: An effective way to harvest microalgae for biodiesel production. *Journal of Environmental Chemical Engineering* **7**, 103221 (2019).

23. Soares, E. V. Flocculation in Saccharomyces cerevisiae: a review: Yeast flocculation: a review. *Journal of Applied Microbiology* **110**, 1–18 (2011).

24. Domingues, L., Teixeira, J. A. & Lima, N. Construction of a flocculent Saccharomyces cerevisiae fermenting lactose. *Appl Microbiol Biotechnol* **51**, 621–626 (1999).

25. Ojima, Y., Nguyen, M. H., Yajima, R. & Taya, M. Flocculation of Escherichia coli Cells in Association with Enhanced Production of Outer Membrane Vesicles. *Applied and Environmental Microbiology* **81**, 5900–5906 (2015).

26. Ojima, Y., Azuma, M. & Taya, M. Inducing flocculation of non-floc-forming Escherichia coli cells. *World J Microbiol Biotechnol* **34**, 185 (2018).

27. Molinari, S., Tesoriero, R. F. & Ajo-Franklin, C. M. Bottom-up approaches to engineered living materials: Challenges and future directions. *Matter* **4**, 3095–3120 (2021).

28. Nguyen, P. Q., Courchesne, N. M. D., Duraj-Thatte, A., Praveschotinunt, P. & Joshi, N. S. Engineered Living Materials: Prospects and Challenges for Using Biological Systems to Direct the Assembly of Smart Materials. *Advanced Materials* **30**, 1704847–1704847 (2018).

29. Chao, G. *et al.* helixCAM: A platform for programmable cellular assembly in bacteria and human cells. *Cell* **185**, 3551-3567.e39 (2022).

30. Glass, D. S. & Riedel-Kruse, I. H. A Synthetic Bacterial Cell-Cell Adhesion Toolbox for Programming Multicellular Morphologies and Patterns. *Cell* **174**, 649-658.e16 (2018).

31. Nguyen, P. Q., Botyanszki, Z., Tay, P. K. R. & Joshi, N. S. Programmable biofilm-based materials from engineered curli nanofibres. *Nature Communications* **5**, 4945 (2014).

32. Roberts, S., Dzuricky, M. & Chilkoti, A. Elastin-like polypeptides as models of intrinsically disordered proteins. *FEBS Letters* **589**, 2477–2486 (2015).

33. Molinari, S. *et al.* A de novo matrix for macroscopic living materials from bacteria. *Nat Commun* **13**, 5544 (2022).

34. Pasotti, L. *et al.* Design of a stable ethanologenic bacterial strain without heterologous plasmids and antibiotic resistance genes for efficient ethanol production from concentrated dairy waste. *Biotechnology for Biofuels and Bioproducts* **16**, 57 (2023).

35. Bird, J. E., Marles-Wright, J. & Giachino, A. A User's Guide to Golden Gate Cloning Methods and Standards. *ACS Synth Biol* **11**, 3551–3563 (2022).

36. Trunk, T., Khalil, H. S. & Leo, J. C. Bacterial autoaggregation. *AIMS Microbiol* **4**, 140–164 (2018).

37. Pasotti, L. *et al.* Engineering endogenous fermentative routes in ethanologenic *Escherichia coli* W for bioethanol production from concentrated whey permeate. *New Biotechnology* **57**, 55–66 (2020).

38. Meyer, D. E. & Chilkoti, A. Genetically Encoded Synthesis of Protein-Based Polymers with Precisely Specified Molecular Weight and Sequence by Recursive Directional Ligation: Examples from the Elastin-like Polypeptide System. *Biomacromolecules* **3**, 357–367 (2002).

39. Liu, H., Chittur, P. K., Kornfield, J. A. & Tirrell, D. A. Cohesive Living Bacterial Films with Tunable Mechanical Properties from Cell Surface Protein Display. *ACS Synth. Biol.* **13**, 3686–3697 (2024).

40. Zakeri, B. *et al.* Peptide tag forming a rapid covalent bond to a protein, through engineering a bacterial adhesin. *PNAS* **109**, E690–E697 (2012).

41. Dubendorf, J. W. & Studier, F. W. Controlling basal expression in an inducible T7 expression system by blocking the target T7 promoter with lac repressor. *Journal of Molecular Biology* **219**, 45–59 (1991).

42. Arunachalam, K. & Sreeja, P. S. Flow Cytometry Protocols for Assessing Membrane Integrity, Cell Cycle, and Apoptosis in Treated Cells. in *Advanced Cell and Molecular Techniques* 195–199 (Springer US, New York, NY, 2025).

43. Rosenberg, M., Azevedo, N. F. & Ivask, A. Propidium iodide staining underestimates viability of adherent bacterial cells. *Sci Rep* **9**, 6483 (2019).

44. Schmidtchen, A., Pasupuleti, M. & Malmsten, M. Effect of hydrophobic modifications in antimicrobial peptides. *Advances in Colloid and Interface Science* **205**, 265–274 (2014).

45. Stevens, A. M. & Greenberg, E. P. Quorum sensing in Vibrio fischeri: essential elements for activation of the luminescence genes. *Journal of Bacteriology* **179**, 557–562 (1997).

46. Gustavsson, M., Bäcklund, E. & Larsson, G. Optimisation of surface expression using the AIDA autotransporter. *Microbial Cell Factories* **10**, 72 (2011).

47. Lupino, K. M. *et al.* A Recurrent Silent Mutation Implicates fecA in Ethanol Tolerance by Escherichia coli. *BMC Microbiol* **18**, 36 (2018).